Mechanical Properties of Microspheres Assembled from Carboxylated Cellulose Nanocrystal Rods

Junqi Wu, and Mark P. Andrews *

J. Wu, Prof. M. Andrews

Department of Chemistry, McGill University, 801 Sherbrooke St W, Montreal, QC, H3A 0B8, Canada

E-mail : mark.andrews@mcgill.ca

Abstract

The elastic modulus of carboxylated cellulose nanocrystal (cCNC) microbeads made by spray-drying were measured by Atomic Force Microscopy (AFM) combined with a 1 μm Si microsphere probe method. Use of a Si microsphere on the cantilever probe tip to measure deformations of cCNC microbeads is shown to eliminate spurious contributions from localized mechanical responses that plague conventional cantilever sharp probe tips. The findings are consistent with the Hertz model. The the Young's modulus of cCNC microbeads depends on spray drying parameters. Spray drying from dilute cCNC suspensions yields particles with a Young's modulus of 18.02 MPa. Higher cCNC feed concentrations yield denser particles characterized by an elastic modulus of 24.55 MPa. Doping dilute cCNC suspensions with citric acid results in aerosol-phase esterification and crosslinking of the cCNC microbeads. Crosslinking in this manner yields a stiffer microbead with a Young's modulus of 27.97 MPa. cCNC-derived microbeads are stiffer than microbeads derived from collagen, hyaluronic acid, alginate, dextran or pectin, but they are more elastic than urethane-acrylate crosslinked beads, and cellulose beads reconstituted from dissolved cellulose by emulsion-precipitation.

Introduction

The mechanical properties of spherical objects like microspheres are essential to understand their performance during manufacture, processing and end-use. Microspheres are generally made from organic polymers, silicates, and other materials, though rarely are they

assembled from other nanoparticles. This is because of the difficulty in organizing nanoscale components over many length scales.[1] Packing of nanoscale geometries into larger scale curved structures touches on the long-standing question of how surface curvature and particle geometry are inter-related. Spherical particles will generally optimize packing on a flat surface by conforming to a hexagonal lattice. Curved surfaces, however, introduce frustration and defects for sphere packing. Spherical packing, but with surface defects, can also occur by replacing spheres with rod-like particles. In this regard, Liu et al. showed how micrometer-size rigid $CaCO_3$ rods will self-assemble on the curved surfaces of bubbles to give highly stable foams.[2] In effect, the $CaCO_3$ rod packing belongs to the paradigm of geometrically frustrated assemblies. Frustration means that local packing motifs can become favoured that do not reflect the uniform global order that might otherwise be assumed by the assembly. Geometric frustration can then yield anomalous structural and thermodynamic properties including heterogeneous and internally stressed equilibrium and non-equilibrium structures. Under certain conditions, rod-like high aspect ratio cellulose nanocrystals (CNCs) in water constitute a canonical self-assembling system. Indeed, CNCs will form a chiral nematic liquid crystalline phase at sufficiently high concentrations of the rigid rods. But what happens when CNC rods are concentrated in water but not allowed to reach thermodynamic equilibrium as they are forced into a curved space? As shown in Figure 1, this situation obtains when CNC rods self-associate but whose liquid crystal order is frustrated inside rapidly evaporating liquid water droplets, a condition that is achieved by spray-drying aqueous CNC feed suspensions. The question of shape and mechanical properties for cCNC microspheres becomes important for microbeads assembled from cellulose nanorods, especially if they are to find applications like those described next.

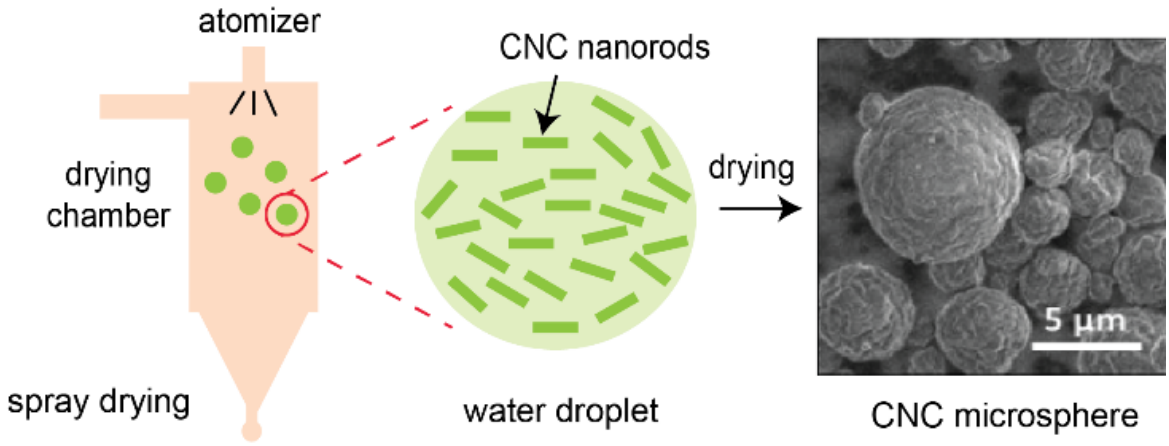

Figure 1. Formation of CNC microspheres from CNC nanorods by spray drying.

Microbeads are commonly used as carriers for drug delivery,[3, 4] in cosmetics and personal care products,[5] as catalysts,[6] and as fillers for cement and concrete.[7] The mechanical properties of microbeads play important roles in several respects. For instance, knowledge of mechanical properties can be used for quality control when manufacturing microbeads,[8] and in a broader sense to identify structure-function-property relationships germane to specific applications of the microparticles.[9,10] In drug delivery systems, the mechanical properties of microbeads determines its capacity survive the stress created during inhalation. Mechanical stability also is important to the reusability of microbeads as catalysts for heterogeneous reactions. As concrete fillers, the elasticity of microbeads and the change of elasticity are the keys to the strength and stability of the concrete.[11] In the cosmetics and personal care industries, microbeads are extensively used to enhance sensory properties in powder formulations.[12] In the latter instance, microbeads impart a variety of benefits, including improved product blending, and enhanced skin feel. All of these require that microbeads be mechanically strong and stable. In short, knowledge of mechanical behavior is important because beads may have to withstand mechanical stress caused by compression when co-processed for inclusion in composite media like foods, structural composites or in pharmaceuticals.

Cellulose is widely regarded as the most abundant natural polymer in the world.[13] Its broad applications are highlighted by the fact that it is non-toxic, biodegradable, renewable as a resource, and admits a mature organic functional group chemistry. While cellulose

microbeads can be produced by membrane emulsification of native cellulose dissolved in an organic electrolyte,[14] spray-drying can be viewed as a competitive alternative that has greater potential to create uniquely cCNC-derived microbeads that retain the native type I cellulose crystallinity. Owing to surface hydroxyl and carboxylate moieties, cCNC has a propensity to form stable nanocrystallite agglomerates in microbeads via hydrogen bonding and van der Waals interactions. Recent research has shown that spray-dried cCNC-derived microbeads will remove dye molecules from waste water.[15] The cCNC-based microbead builds on the strength of the high crystallinity index of cellulose. Indeed, cellulose nanocrystals show a Young's modulus as high as 100 GPa.[16] To advance applications of CNC-derived microbeads, measurement of their mechanical properties is important in order to understand microbead structure-function relationships in order to design strategies for tailoring mechanical properties to fit specific applications.

Mechanical property measurements include elasticity, viscoelasticity, hardness, and fatigue limit. The literature typically focuses on single bead and ensemble assessments. Among mechanical properties, the Young's modulus measures the stiffness of materials. The modulus is defined as the ratio of stress along an axis to strain along the same axis in response to uniaxial loading.[17] It can be used to measure the resistance of a microbead to elastic deformation under load; however, measurement of the Young's modulus of microbeads remains challenging.

The force generated from traditional mechanical testing machines is too large to probe microbead deformation: for microbeads, a reasonable deformation requires forces within the micro-newton range.[18] Scott et al. used a compression test to measure the compressibility of non-crosslinked and crosslinked cellulose microbeads. Crosslinked cellulose microbeads show an increase in mechanical strength, but also an increase in brittleness.[14] The Scott method measures the mechanical properties of loosely-packed powders. In this case, interactions among microbeads may compromise the measurement results. Several methods have been developed to measure single microbeads. Micromanipulation provides mechanical perturbation to small structures using microplates or probes connected to force transducers. The method enables the real-time observation of specimen deformation. But the set-up can be complicated.[19] Micropipette aspiration,[20, 21]

and optical tweezers[22] have been used to measure the mechanical properties of micro-sized objects. But these techniques are used mainly for cell deformation measurements because the force range is often insufficient to induce any significant deformation in other types of microbeads. Ngan et al. proposed a microplate compression method to probe the viscoelastic mechanical properties of a hydrogel collagen microbead.[18] Shimadzu Corporation has commercialized the micro-compression test machine to measure softness and elasticity.[23]

Nanoindentation is one approach to measure the mechanical properties of small spheres.[24] Nanoindentation is usually performed with a nano-indenter or by AFM. AFM offers a quantitative, programmable, and repeatable method for microbead mechanical properties measurement over a wide range of particle sizes.[25-28] Because the indenter tip size is significantly smaller than the size of a microparticle, the modulus can vary significantly as the tip interrogated the surface .[9, 18] Recently, Li et al. have described the use of AFM to measure the mechanical properties of ~500 μm diameter regenerated cellulose microbeads. Those beads were prepared via the conventional method of complete dissolution of cellulose into a polymer chain disperse phase in LiCl/DMAc liquid. [29] In this measurement, spherical gold particles were used as indentation probes. The mechanical properties were compared with different hydration status of the beads. Here in our paper, we intend to use similar methodology to test the mechanical elasticity of dry microspheres assembled from cellulose nanocrystal rigid rods.

We have adapted a method to measure cellulose microbead stiffness by AFM to provide more accurate determination of the Young's modulus when compared with the use of a conventional sharp tip. In this paper we measure how small molecule crosslinker affects the mechanical properties of cCNC microbeads. cCNC microbeads with porous internal structure and solid internal structure are also compared. Finally, we compare the elasticity of cCNC microbeads to commercial cellulose and other classes of microbeads. We show that AFM mechanical measurements are a promising approach to quantify the elastic response of soft microbeads.

Experimental Procedures

2.1. Materials

cCNC (5.3 wt % suspension in water) and ChromaPur Neige® 2B cCNC microspheres were donated by Anomera Inc., Montreal, Canada. ChromaPur Neige 2B is a product spray dried from CNC >4 wt% water suspension (American Custom Drying, Burlington, New Jersey). Cellulose D-5 cellulose microbeads prepared by emulsion precipitation, were obtained from Kobo Products, Inc. Marsh Mallow Powder (Average size: 9.8 μm) was obtained from Sunjin Beauty Science (INCI (International Nomenclature of Cosmetic Ingredients) Name: Hexamethylene diisocyanate/Trimethylol Hexyllactone Crosspolymer).

2.2. Spray-drying

Spray-drying was carried out with a Büchi Mini Spray Dryer B-191 (Büchi Corporation, New Castle, USA) with inlet and outlet temperatures of 175 °C and 104 °C, respectively, 30% pump speed and 70% aspirator. cCNC microbeads were made by spray-drying cCNC 0.5 wt % from distilled water. Citric acid (CA) containing microbeads were made by spray-drying the aqueous cCNC suspension (0.5 wt %) mixed with 10% CA.

2.3. SEM

SEM was conducted using an FEI Quanta 450 Environmental Scanning Electron Microscope on samples coated with 3 nm of platinum.

An FEI Helios Nanolab 660 DualBeam (Focused Ion Beam-Extreme High-Resolution Scanning Electron Microscope) was used for cCNC-based microbead cross-section imaging. The samples were mounted on an aluminum SEM stub and coated with a 4 nm layer of Pt to enhance electrical conductivity. Milling of the sample was carried out with an FEI Helios Nanolab 660 DualBeam instrument (Thermo Fisher Scientific, Hillsboro, OR USA). After selecting a specific particle, a 2 micron thick of protective platinum stripe was deposited on the surface of the region of interest to protect the surface from ion beam damage. Microbead cross-sections were then prepared by gallium ion milling. A primary trench to clean the sample was milled at 30 kV ion beam accelerating voltage and 21 nA beam current. Following cleaning, cross-sections were obtained with beam current ranging between 9.3 nA to 0.79 nA. The smooth cross-section was imaged with an electron beam

at an accelerating voltage of 2 kV, a beam current of 0.40 nA, and a working distance of 4 mm in the secondary electron mode.

2.4. Sample Preparation

Separate samples of cCNC (produced from 0.5% suspension), 10% CA, Marsh Mallow powder, and ChromaPur Neige 2B were dispersed in water. Each the mixture was cast separately on a freshly cleaved mica substrate and dried at ambient conditions overnight before conducting AFM nanoindentation.

2.5. Calibration of the AFM Cantilever Spring Constant k

The spring constant of the cantilever was measured by taking into account contributions due to thermal noise according to the procedure of Butt and Jaschke.[30] A force curve was first obtained on a glass substrate, and the slope of the approaching curve measured to determine the sensitivity of the cantilever. Then the AFM tip was removed far from the surface so that oscillations were determined only by the thermal noise of the cantilever. In this way, power spectra were collected. The power spectral density of the fluctuations in the spring displacement was fit to a Lorentzian, and the resonance frequency extracted. The calculation of the spring constant follows Equation (1):

$$k = k_B T / P \quad (1)$$

where P is the area of the power spectrum of the thermal fluctuations alone, T is the Temperature, k_B is Boltzmann's constant.

2.6. Mechanical Properties Measurement by AFM

Mechanical property analysis was conducted in air under ambient conditions with a commercial AFM MFP - 3D - BIO AFM instrument (Asylum Research, Santa Barbara CA). Ffiand microbead surface morphology imaging (coated with reflective Aluminium on the backside). Biosphere B500-FM cantilevers (Nanotools USA LLC, Henderson, NV) with a spring constant of k = 2.8 N/m were equipped with Si particle with a radius of 500 nm. The microsphere probe was used for force measurement. Topographic images were first acquired to identify the center positions of the microbeads and measure the sizes of individual microbeads. To investigate the mechanical properties of individual microbeads

at a well-defined location, a "point and shoot" view was used. After scanning over individual microbeads in a given area, around 100 microbeads were selected from the topographic image. A crosshair was used to target the center of a microbead for force curve collection. The mechanical properties of the microbeads were obtained by analyzing the force-distance curves. For force measurement, a contact mode was used with a trigger point of 2 V, force distance of 1 μm, scan rate of 0.99 Hz, and velocity of 1.98 μm/s. For topographic images, the AC mode was conducted with 20 μm scan size, 0.8 Hz scan rate. We excluded force curves in those cases where the Young's modulus was comparable to the substrate. We also excluded force curves that indicated anomalously low stiffness. This happens when the probe is not indenting the microbeads, but creating a lateral motion rather than a sphere deformation.

2.7. Elastic Modulus Modeling

Three theoretical models are may be used to model tip-sphere contact: Hertzian elastic,[25, 26, 28] Johnson-Kendall-Roberts (JKR),[26, 28, 31-33] and Derjagui-Muller-Toporov (DMT).[34] The widely used Hertzian elastic model describes perfect elastic deformation between two spherical bodies in contact, without considering the adhesion force. The JKR and DMT models describe an elastic-plus-adhesive contact. The latter are used when it is evident that adhesion plays a significant role in the elastic response. Our calculation of the Young's modulus E follows from the Hertz model in equation (2) and equation (3). We used the Poisson's ratio υ of bulk cellulose (0.38) for the calculation.[35] The AFM silicon tip has an elastic modulus of 130 - 160 GPa and Poisson's ratio of 0.27. The tip deformation is negligible due to the significantly higher stiffness of the tip compared with cellulose target.[36]

$$F_{sphere} = \frac{4}{3}\frac{E}{1-v^2}\sqrt{R}\delta^{\frac{3}{2}} \qquad (2)$$

$$E = \frac{3}{4}\left(\frac{\Delta\left(F_{sphere}\right)^{2/3}}{\Delta\delta}\right)^{3/2} \frac{1-v^2}{\sqrt{R}} \quad (3)$$

2.8. Data Processing

Force-displacement curves were converted into the force-indentation curves to quantify the elastic modulus. This was accomplished with AFM MFP-3D-BIO AFM instrument software. MATLAB code (in supporting information) was written to extract elasticity and fitting parameters based on the Hertz Model. For this, we used the retracing part of a series of force curves. Up to 100 curves were collected using the method described in 2.6.

Results and discussion

3.1. The Contact Model for Young's Modulus

We first calibrated the microsphere probe method with polystyrene microbeads. The calculated Young's modulus (~1.16GPa) is within the range of values reported in the literature (Figure S1).

We justify our use of the Hertzian model as follows: Figure 2 (a) presents a force-indentation curve for cCNC microbeads. The average indentation depth is less than ~~inside~~ 25 nm. This agrees with the literature consensus that the indentation depth should fall within 10% of the total depth so that the substrate does not influence the deformation measurement.[37 38, 39] The adhesion force can contribute to the elastic response of microbead mechanical property measurements, especially at low indentation depth. Sarrazin *et al.* have shown that the adhesion force influences the measured Young's modulus for indentations < 2 - 5 nm. Increasing the indentation depth to more than 5 nm ensures that elastic bulk effects dominate, and the adhesion force can be regarded as negligible.[26] For these reasons we justified selection of the Hertzian model, which depends on a linear fit to the indentation depth expressed as $\delta^{3/2}$.[40] As shown in Figure 2 (b), $\delta^{3/2}$ is linear with respect to force (coefficient of determination of 0.997), justifying our choice of the Hertz model.

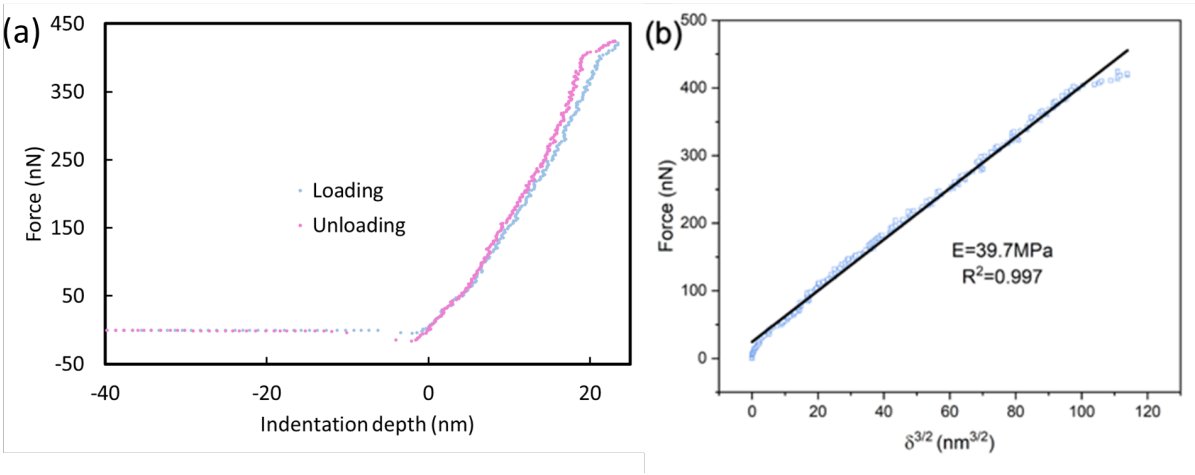

Figure 2 Fits to the Hertz model to determine the Young's modulus of cCNC microbeads using a nanosized AFM probe. (a) One representation of force-indentation curve for cCNC microbeads using the FMV-A cantilevers (Bruker Nano Inc.). (b) Fit of the Hertz model to determine the Young's modulus.

We deposited cCNC microbeads on a freshly-cleaved Muscovite mica substrate to measure mechanical properties. A topographical scan was repeated in the measurement area to ensure the particles remained fixed after indentation (Figure S2). On the mica substrate, the microbeads indeed remained fixed before and after indentation. No damage to the microbeads, such as a surface depression, was detected after indentation, indicating no viscoplastic response. This is important since plastic deformation of particles is inconsistent with assumptions in the Hertz model.

3.2. Comparison of AFM Indentation on cCNC Microbeads using AFM Nanoprobes and Microsphere Probes

We first measured the Young's modulus by conventional tip based AFM in order to compare our findings with those obtained by the microsphere probe method. Figure 3 (a) shows the results from a conventional tip, a nano-scale probe. With the method described in the experimental section, we extracted the force curves by indenting more than 100 microbeads. After fitting the force curves to the Hertz model, the Young's modulus was calculated. Figure 3 (c) shows the results accumulated from 50 force curves after rejecting the spurious curves. With a conventional tip, the Young's moduli vary widely, from 20 MPa to 2 GPa (Figure 3(c)). Clearly, measurement of local mechanical properties with a

sharp tip may not represent the mechanical deformation of a microbead as a whole. As shown in Figure 3 (a), when approaching the surface of a cCNC microbead with an AFM tip of 8 nm radius of curvature, the force curves generated are location-dependent due to the nanoporous structure of the cCNC microbeads, curvature and the gaps among beads (location offset). For example, location 1 in Figure 4 (a) probes cCNC crystallites, giving a significantly high value of elasticity. Location 2 probes the gaps between the crystals, showing a relatively low elasticity. This phenomenon results in a broad range of elasticity outcomes, as shown in Figure 3 (c), making AFM indentation for porous microbeads unreliable because one cannot predict where the tip lands on a microbead surface.

A second drawback when using a nano-radius tip is that damage to the probe tip changes its radius, R. The impact on mechanical measurements can be significant when calculating the Young's modulus because the modulus depends on $\sqrt{R}$. In Figure 3 (a), we imaged the tip radius of nano-scale probes before and after nanoindentation. The radius R of the tip increased from 8 nm to ~20 nm. The change in tip size produces significant error in determining the modulus. Guo et al.[28] have studied tip wear and its effect on measured Young's modulus values. They concluded that a tip with a smaller radius of curvature is more likely to induce location offset on the substrate, giving rise to tip wear.[41] Therefore, a larger radius of curvature, like a microsphere, is recommended for mechanical measurements.

Thirdly, the Hertz model describes elastic deformation between two perfect spheres. It is most accurate when the two spheres have the same radius. Using a nano-sized probe gives less accurate Hertz fitting because of the significant difference in radius between the radius of AFM tip and cCNC microbeads.[42]

When indenting microbeads with microsphere probes, we overcome the limitations of nano-sized tips described above. Figure 3 (d) shows the Young's modulus measured using this microsphere probe tip. The tip yields a good Gaussian distribution of elasticity results with decreased measurement errors. The average Young's modulus is 18.02 MPa with standard deviation of 1.13 MPa. This method is not only able to provide average mechanical properties, but the ability to measure the elasticity of each particle means it also yields the deviation from the mean of mechanical properties. This is significant because most current

indentation methods fail to measure the Young's modulus of single particles, especially for microparticles that are ~ 1-2 µm in size. Philippe *et al.*[43] compared their results with microsphere probe with literature data and concluded that microsphere probe indentation gives a Young's modulus lower than that measured using sharp tips. Our results align with their conclusion. The results from microsphere probes are likely to be more accurate. Since the radius of the nano-sized tip is two orders of magnitude smaller than a microsphere probe, the pressure on a microbead from a nano-scale tip is much higher. The nano-scale tip can also cause local strain hardening,[43] making the Young's modulus results less accurate.

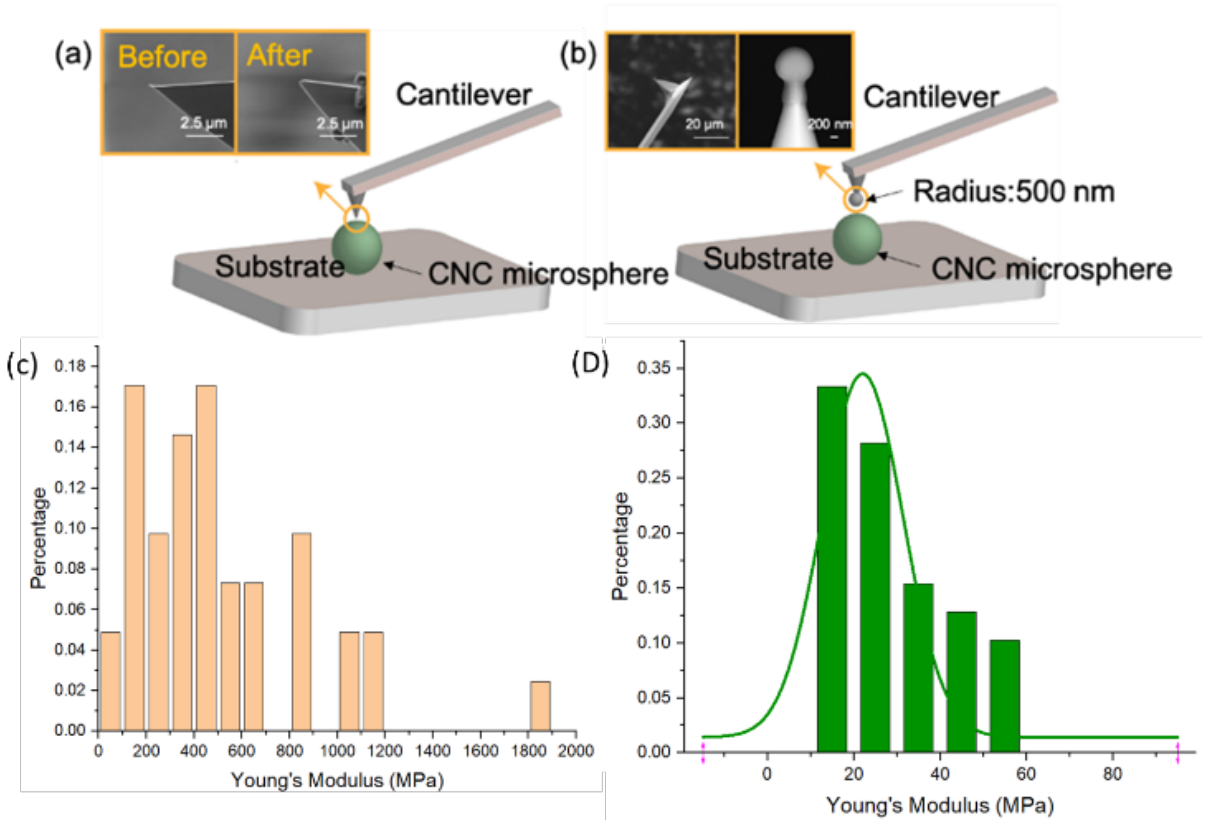

Figure 3. Comparison AFM indentation with a conventional nano-scale tip and microsphere tip. (a) AFM nanoindentation set-up illustration and SEM images of tip used for indentation before and after. (b) AFM indentation set-up illustration with micro-sized tip. (c) Young's modulus of cCNC microbeads calculated from the Hertz model for a nano-

scale tip. (d) Young's modulus of cCNC microbeads calculated from the Hertz model for a microsphere probe. The curve is Gaussian fits to the data.

Figure 4 (a) shows the phase image of a cCNC microbead surface. The surface is porous like a structured foam. The texture is likely the result of the rapid drying and water loss from the aqueous microdroplet during spray-drying. The thickness of the ridges is on the order of the width of 1 to several cCNC rods that are overlapped end to end to yield a fibrous network. The pores have an average value of ~50 nm. Microbeads produced from 0.5 wt % cCNC suspension are ~ 2 μm in diameter, hence, a 1 μm microsphere probe is appropriate for mechanical measurement. We used a 500 nm radius Si probe from Nanotools for the measurement. The probe was fabricated from a silicon microsphere that was eroded by electron beam to a diameter of about 1000 nm. A probe of this size reduces tip wear and the potential of microsphere tip damage during indentation.[44]

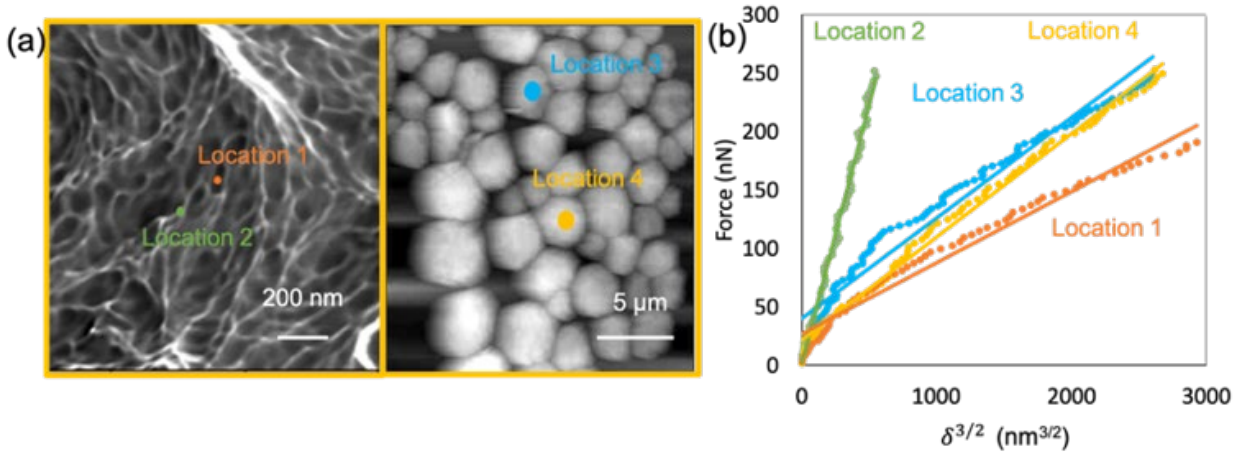

Figure 4 Comparison of AFM indentation using conventional nano-sized tips and microsphere tips. (a) AFM phase image of cCNC microbead surface porous structure with two locations identified for force curve measurement (image on the left) and AFM topographic scanning image of cCNC microbeads with two microbeads identified for two force curves measured (image on the right). (b) Plots of force versus $\boldsymbol{\delta^{3/2}}$ for the locations identified in Figure 4 (a). δ is the indentation depth.

3.3. Enhanced Young's Modulus in Citric Acid Crosslinked cCNC Microbeads

With the microsphere probe method, we explored the effect crosslinking among cCNC particles in microbeads and its impact on the elastic modulus. As described in experimental section, we first scanned to produce topographic AFM images of both cCNC microbeads and 10% CA microbeads to identify the positions of the microbeads. The outcomes are shown in Figure 5 (a) and Figure 5 (b). The red "X" marks the targeted indentation positions. From the topographic image, cCNC microbeads and 10% CA crosslinked microbeads show similar shapes and particle sizes. The force curves were collected and the Young's moduli were calculated. The accumulated results are plotted in Figure 5 (c), where it is evident that inclusion of citric acid increases the modulus to 27.97 MPa compared with that of 18.02 MPa for cCNC without CA. The increase in the modulus is 55% with a loading of 10% CA. For comparison, Reddy *et al.* reported that starch film crosslinked with citric acid exhibited a 150% increase in tensile strength compared with non-crosslinked films.[45] Similarly, Shao *et al.* showed that the tensile strength of citric acid-crosslinked hemicellulose-based films increased by 67% on reaction with 20% CA.[46] Arne *et al.* used citric acid to crosslink nanocellulose to develop robust paper filters.[47] In our case, the vibrational spectra reported in the supplementary sections, SI Figure S3 and Figure S4 prove that crosslinking occurs between CA and the cCNC microbeads. Since the existence of abundant amount of carboxylic acid group (~1700 cm^{-1}) on citric acid may cover the appearance of ester bond (v~1750 cm^{-1}), we pre-treated the microbeads in dilute basic solution (pH=8) to shift carboxylic acid v (C=O) stretch from ~1700 cm^{-1} to sodium carboxylate at ~1650 cm^{-1}. The ester crosslink is illustrated in Figure 5 (d). The implications of the findings are significant. They demonstrate (a) that ester bond formation can take place in one step in the liquid phase in the micro environment of a water droplet generated from spray nozzle of CA and cCNC particles driving by the rapid water evaporation; (b) that the process does not require ancillary agents like anhydrides; (c) that the chemical outcome increases the Young's modulus of the microbead; (d) that a hybrid microbead can be made that comprises "naturally sourced" components; and (e) that the process uses scalable spray-drying. In the following section, we turn to a qualitative interpretation of how some spray-drying parameters determine particle morphology and other features of cCNC powders.

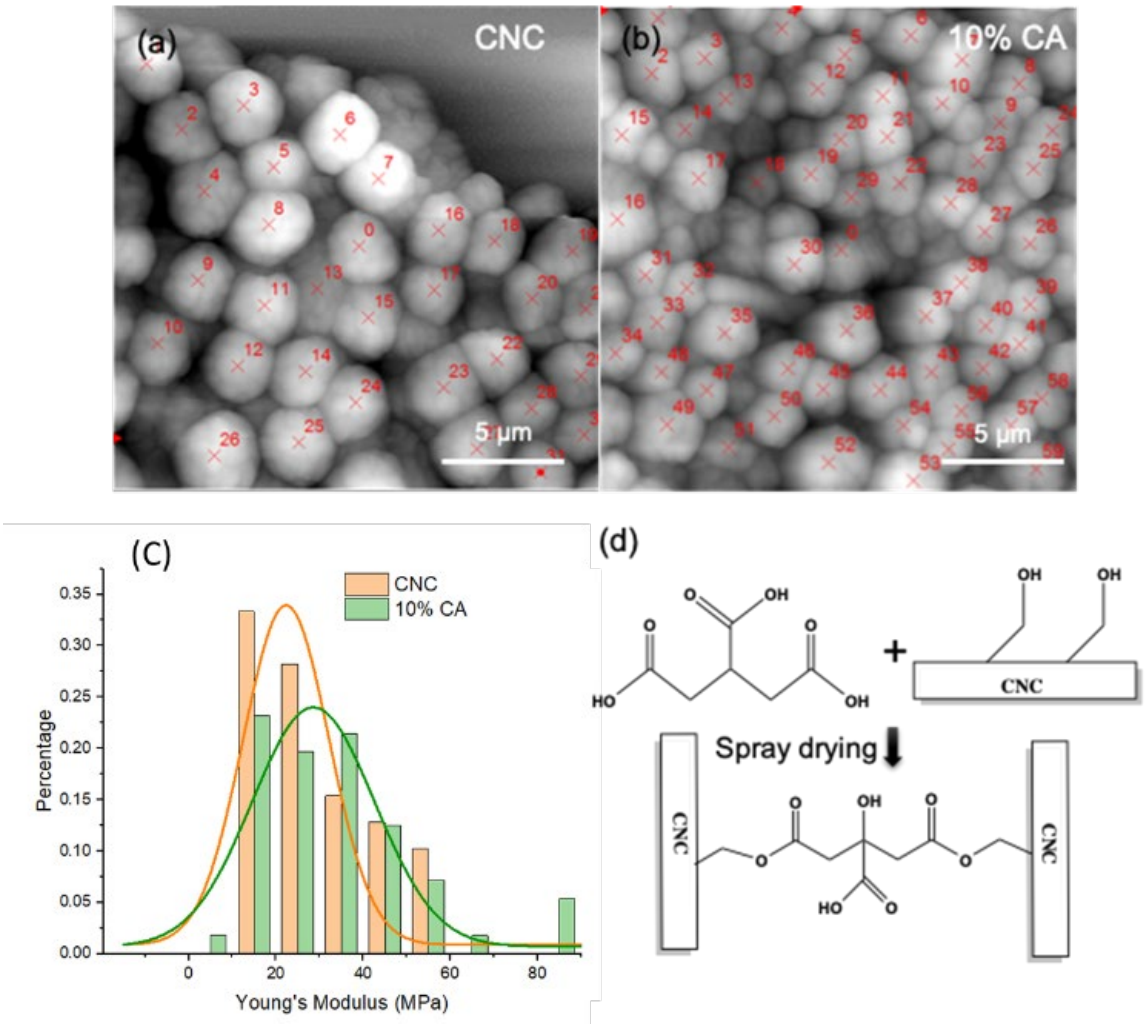

Figure 5. Comparison of Young's modulus of cCNC microbeads and 10% citric acid crosslinked cCNC microbeads. (a) AFM topographic images of cCNC microbeads with red cross marks to identify the center of the indentation. (b) AFM topographic images of 10% CA crosslinked microbeads with red cross marks to identify the center of the indentation. (c) Young's modulus measured for cCNC microbeads and 10% CA microbeads. (d) Illustration of chemical crosslinking between cCNC and citric acid by esterification. The curves are Gaussian fits to the data.

3.4. Mechanical Properties of Porous and Dense cCNC Microbeads

Spray-drying is a one-step, water-based method to make cCNC microbeads. Spray-drying involves multiple process parameters that can influence the properties of the microparticles.[48] For example, the viscosity and concentration of the suspension are control

parameters that can be used to determine particle size and size distribution. The outlet temperature, droplet size and feed concentration affect the morphology of the particles, especially deviations from spherical and dry particle density. Typically, particles tend to be spherical at high evaporation rates and short drying times. Figure 6 (a) is the AFM image of a commercial sample of microbeads prepared from 4.5 wt % cCNC suspensions (ChromaPure Neige 2B) in an industrial scale high throughput dryer. Figure 6 (b) shows an AFM image of cCNC microbeads prepared from 0.5 wt % suspensions in a benchtop Buchi dryer. Microbeads from both spray dryers are roughly spherical. Small differences in nozzle type, back pressure, outlet temperature and throughput lead to a result where shape alone does not tell the whole story. The FIB cross-sections of Figure 6 (c) and Figure 6 (d) for beads from the two types of dryers reveal different internal structure. cCNC microbeads from the 0.5 wt % suspension from the Buchi tool have a porous internal core and a densely packed shell structure. Microbeads from 4.5 wt % suspensions are dense. It seems that spray-drying a higher wt % cCNC suspension produces cCNC microbeads with higher density. Péclet number can be used to determine the impact of particle diffusion and convection on particle morphologies. The competition can be quantified through the dimensionless Péclet number (P_e), defined in Equation (4). In this equation, R is the radius of droplet, t_{dry} is the drying time, and D is the diffusion coefficient of the suspended particles.

$$P_e = \frac{R^2}{D t_{dry}} \tag{4}$$

For a spherical nanoparticle, D can be calculated from the Stokes-Einstein equation (2).

$$D = \frac{k_B T}{6\pi\eta r} \tag{5}$$

where, k_B is the Boltzmann constant, η is the viscosity of the solvent, T is the absolute temperature, and *r* is the effective hydrodynamic radius of a diffusing particle. When the Péclet number is low, diffusion dominates, leading to an evenly distributed particle concentration through the water droplet. During water evaporation, the droplet shrinks, to yield a dense particle, perhaps with irregular surfaces. In contrast, a high Péclet number results in convective transport. In this case, solute accumulates at the air-water interface. We calculated the Péclet number of cCNC to be about 10^{-3} based on a drying time of 6 s, particle radius of 180 nm, and diffusion coefficient D ~ 0.542×10^{-11} m^2/s. The Péclet number here is misleading because it assumes that the

cellulose nanocrystals in the evaporating water droplet are non-interacting, when in fact they gel rapidly as water evaporates, meaning that the diffusion coefficient for cCNC and water are likely to increase rapidly. This would cause a rapid increase in the Péclet number. A high Péclet number promotes spherical shell formation. We theorize that for the 4.5 wt % cCNC suspension, the microbeads are densely packed because the initial Péclet number is already higher to start with. The spray-drying time plays a major role for determining the density of the particles. With higher concentration of cCNC suspensions, the drying time increases, leading to a longer time for nanocrystal aggregation during the water loss phase. Pre-aggregation of the particles in the higher wt % cCNC suspension also contributes to the increase in density of the spray dried particles.

By microsphere probe based AFM nanoindentation the Young's modulus of ChromaPure Neige 2B is 24.55 MPa, compared with a value of 18.02 MPa for microbeads produced from 0.5 wt % suspension with the benchtop spray dryer. The results are shown in Figure 6 (e) and (f). As expected, densely packed cCNC microbeads have a higher Young's modulus than porous particles when other parameters are controlled.

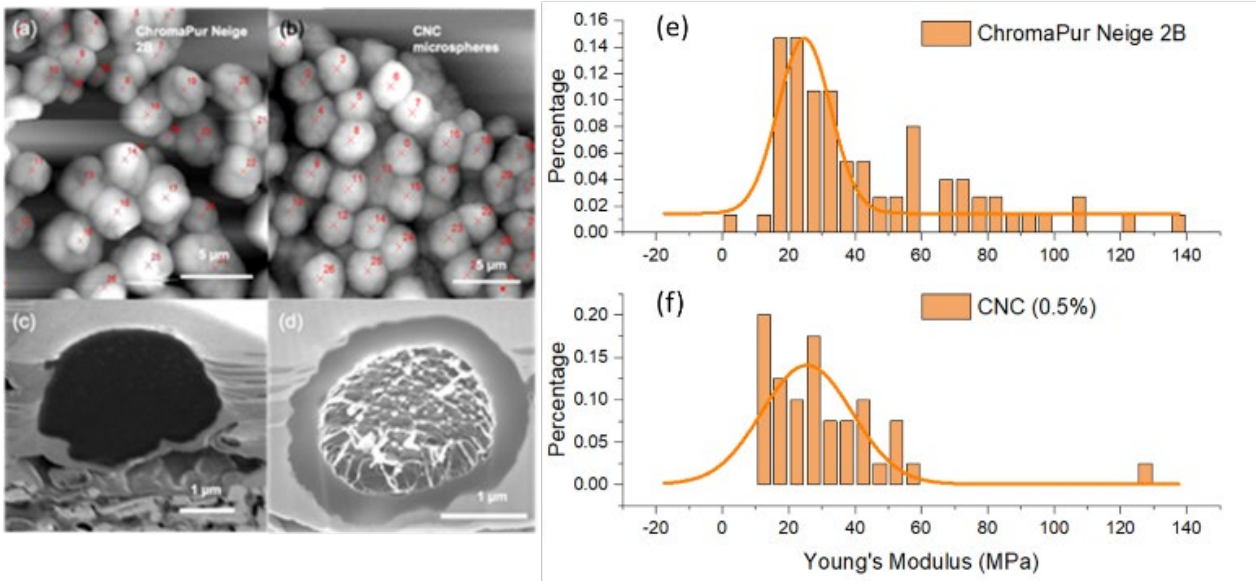

Figure 6. Dependence of Young's modulus on cCNC suspension concentration for spray-drying. (a) ChromaPur Neige 2B AFM AC mode topographic image. (b) cCNC microbeads from 0.5% slurry AFM AC mode topographic image. (c) FIB-SEM image of cross-section of a ChromaPur Neige 2B. (d) FIB-SEM image of cross-section of a cCNC microbead. (e)-

(f) Histogram distribution for Young's modulus of cCNC microbeads and ChromaPur Neige 2B microbeads. The curves are Gaussian fits to the data.

3.5. Comparison with Commercial Beads Made from Soft Materials

Several commercial beads are available for use in non-wash-off cosmetics. Examples are the Marsh Mallow powder from Sunjin Beauty Science and Cellulose D-5 from Daito Kasei. We now compare the Young's modulus (elasticity) of our cCNC microbeads with the commercially available ones. Figure 7 shows the Young's modulus of several microbead powders measured using the same method: cCNC produced from 0.5 wt % cCNC suspension, ChromaPure Neige 2B (Anomera), 10% CA, cellulose D-5 (Daito Kasei) and Marsh Mallow (Sun Jin). The cellulose D-5 microbead is a ~10 µm amorphous cellulose particle prepared by dissolving native cellulose in strongly basic media, followed by emulsification/precipitation. The Marsh Mallow powder is a crosslinked urethane-acrylate plastic microbead. With the exception of silica, plastic microbeads like the Marsh Mallow product, are mechanically stiff compared with the cellulosic microbeads. The amorphous D-5 cellulose microbead is approximately twice as stiff as those derived from carboxylated cellulose nanocrystals.

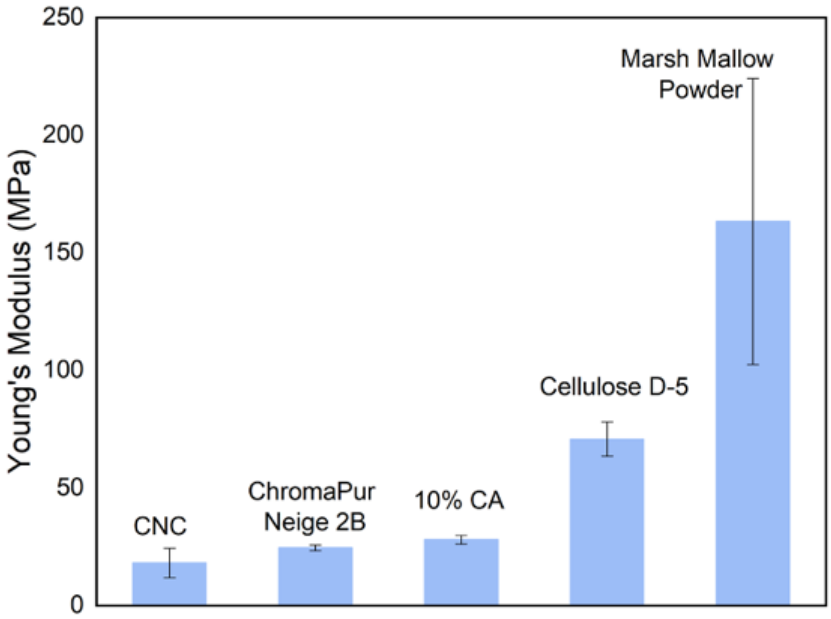

Figure 7. Young's Modulus of available commercial beads Cellulose D-5 and Marsh Mallow Powder comparison with cCNC-based microbeads.

Conclusions

Spherical cellulose microbeads can be prepared from cellulose nanocrystal rods by quench assembly in evaporating water aerosol microdroplets. This unusual example of microsphere growth from nanoparticles invites examination of their mechanical properties. In particular, the Young's modulus of cCNC-based microbeads was determined by an AFM microsphere probe nanoindentation method. The method is an improvement over conventional tip based AFM nanoindentation. The Hertz model was shown to yield reliable data over many samples of individual microbeads. Microbeads from CNC nanorods are stiffer than microbeads prepared from dextran, hyaluronic acid, alginate, collagen, or pectin. The nanorod-based microspheres are "softer" than a commercial cellulose bead prepared by the viscose process, and considerable softer than a commercial plastic microbead. The Young's modulus of neat cCNC microbeads depends on the process of spray drying. Beads prepared with a benchtop dryer yield porous microbeads with a Young's modulus of ~18.02 MPa. Beads prepared in a commercial spray dryer are dense particles with a modulus of 24.55 MPa. Crosslinking of CNC with citric acid raises the modulus to 27.97 MPa. Crosslinking occurs by aerosol phase esterification during quench condensation of the nanorods to make the spherical microbead. Future work will examine the mechanical response of cCNC microbeads in various solvent environments, under humid conditions (hydration), and when combined with other functional polymeric systems.

Conflicts of interest

The authors declare no conflict of interest.

Acknowledgments

We gratefully acknowledge financial support from the Natural Science and Engineering Research Council (NSERC) of Canada RGPIN-2018-05912, the Quebec Centre of Advanced Materials/Centre Québécois sur les Matériaux Fonctionnels (QCAM/CQMF), and the McGill Sustainability Systems Initiative (MSSI) MSSI 172703. The McGill Institute from Advanced Materials (MIAM) and the McGill Facility for Electron Microscopy Research (FEMR) provided support in the way of sample characterization. cCNC microbeads and suspensions were kindly donated by Anomera Inc.

References

1. M. S. Wong, J. N. Cha, K.-S. Choi, T. J. Deming and G. D. Stucky, *Nano Letters*, 2002, **2**, 583-587.
2. W. Zhou, J. Cao, W. Liu and S. Stoyanov, *Angewandte Chemie*, 2009, **121**, 384-387.
3. K. Saralidze, L. H. Koole and M. L. W. Knetsch, *Materials*, 2010, **3**, 3537-3564.
4. K. M. Z. Hossain, U. Patel and I. Ahmed, *Progress in biomaterials*, 2015, **4**, 1-19.
5. F. Casanova and L. Santos, *Journal of Microencapsulation*, 2016, **33**, 1-17.
6. Y. Liu, J.-F. Chen, J. Bao and Y. Zhang, *ACS Catalysis*, 2015, **5**, 3905-3909.
7. V. Semenov and T. Rozovskaya, *Procedia Engineering*, 2016, **153**, 623-629.
8. R. Mercadé-Prieto and Z. Zhang, *Journal of Microencapsulation*, 2012, **29**, 277-285.
9. M. Lekka, D. Sainz-Serp, A. J. Kulik and C. Wandrey, *Langmuir*, 2004, **20**, 9968-9977.
10. F. Jiang, T. Huang, C. He, H. R. Brown and H. Wang, *The Journal of Physical Chemistry B*, 2013, **117**, 13679-13687.
11. A. Aruniit, J. Kers, J. Majak, A. Krumme and K. Tall, *Proceedings of the Estonian Academy of Sciences*, 2012, **61**.
12. H. Leslie, *Institute for Environmental Studies [IVM]*, 2014, **4**.
13. C. Brigham, in *Green Chemistry*, eds. B. Török and T. Dransfield, Elsevier, 2018, DOI: https://doi.org/10.1016/B978-0-12-809270-5.00027-3, pp. 753-770.
14. J. Coombs Obrien, L. Torrente-Murciano, D. Mattia and J. L. Scott, *ACS Sustainable Chemistry & Engineering*, 2017, **5**, 5931-5939.
15. EP15826572.8A, 2016.
16. S. Iwamoto, W. Kai, A. Isogai and T. Iwata, *Biomacromolecules*, 2009, **10**, 2571-2576.
17. M. Pyke, in *Structural Chemistry of Glasses*, ed. K. J. Rao, Elsevier Science Ltd, Oxford, 2002, DOI: https://doi.org/10.1016/B978-008043958-7/50028-5, pp. 401-427.
18. B. P. Chan, C. H. Li, K. L. Au-Yeung, K. Y. Sze and A. H. W. Ngan, *Annals of Biomedical Engineering*, 2008, **36**, 1254-1267.
19. Y. Harada, T. Ota and T. Takamatsu, 2007.
20. Y. Lefebvre, E. Leclerc, D. Barthès-Biesel, J. Walter and F. Edwards-Lévy, *Physics of Fluids*, 2008, **20**, 123102.
21. Y.-J. Li, Y.-N. Yang, H.-J. Zhang, C.-D. Xue, D.-P. Zeng, T. Cao and K.-R. Qin, *Micromachines*, 2019, **10**, 131.

22. Y. Tan, D. Sun, J. Wang and W. Huang, *IEEE Transactions on Biomedical Engineering*, 2010, **57**, 1816-1825.
23. S. Fujisawa, E. Togawa, K. Kuroda, T. Saito and A. Isogai, *Nanoscale*, 2019, **11**, 15004-15009.
24. S. Kim, Y. Lee, M. Lee, S. An and S.-J. Cho, *Nanomaterials*, 2021, **11**, 1593.
25. S. Tan, R. L. Sherman and W. T. Ford, *Langmuir*, 2004, **20**, 7015-7020.
26. B. Sarrazin, N. Tsapis, L. Mousnier, N. Taulier, W. Urbach and P. Guenoun, *Langmuir*, 2016, **32**, 4610-4618.
27. A. J. Svagan, A. Musyanovych, M. Kappl, M. Bernhardt, G. Glasser, C. Wohnhaas, L. A. Berglund, J. Risbo and K. Landfester, *Biomacromolecules*, 2014, **15**, 1852-1859.
28. D. Guo, J. Li, G. Xie, Y. Wang and J. Luo, *Langmuir*, 2014, **30**, 7206-7212.
29. H. Li, K. Mystek, L. Wågberg and T. Pettersson, *Soft Matter*, 2020, **16**, 6457-6462.
30. H. J. Butt and M. Jaschke, *Nanotechnology*, 1995, **6**, 1-7.
31. L.-Y. Lin and D.-E. Kim, *Polymer Testing*, 2012, **31**, 926-930.
32. Y. M. Efremov, D. V. Bagrov, M. P. Kirpichnikov and K. V. Shaitan, *Colloids and Surfaces B: Biointerfaces*, 2015, **134**, 131-139.
33. V. V. Tsukruk, Z. Huang, S. A. Chizhik and V. V. Gorbunov, *Journal of Materials Science*, 1998, **33**, 4905-4909.
34. J. Hellwig, R. M. P. Karlsson, L. Wågberg and T. Pettersson, *Analytical Methods*, 2017, **9**, 4019-4022.
35. K. I. Nakamura, M. Wada, S. Kuga and T. Okano, *Journal of Polymer Science Part B: Polymer Physics*, 2004, **42**, 1206-1211.
36. A. Vinckier and G. Semenza, *FEBS Letters*, 1998, **430**, 12-16.
37. X. Xi, S. H. Kim and B. Tittmann, *Journal of Applied Physics*, 2015, **117**, 024703.
38. J. Chen and S. J. Bull, *Vacuum*, 2009, **83**, 911-920.
39. W. Zhang, J. Li, Y. Xing, X. Nie, F. Lang, S. Yang, X. Hou and C. Zhao, *Coatings*, 2021, **11**, 23.
40. M. Asgari, *Soft Matter*, 2017, **13**, 7112-7128.
41. E. Broitman, *Friction*, 2014, **2**, 40-46.

42. A. R. Ingraffea and P. A. Wawrzynek, in *Comprehensive Structural Integrity*, eds. I. Milne, R. O. Ritchie and B. Karihaloo, Pergamon, Oxford, 2003, DOI: https://doi.org/10.1016/B0-08-043749-4/03007-X, pp. 1-88.
43. P. Carl and H. Schillers, *Pflügers Archiv - European Journal of Physiology*, 2008, **457**, 551.
44. S. Schmidt, J. Foucher, C. Penzkofer and B. Irmer, *Controlled fabrication of advanced functional structures on the nanoscale by means of electron beam-induced processing*, 2013.
45. N. Reddy and Y. Yang, *Food Chemistry*, 2010, **118**, 702-711.
46. H. Shao, H. Sun, B. Yang, H. Zhang and Y. Hu, *RSC Advances*, 2019, **9**, 2395-2401.
47. A. Quellmalz and A. Mihranyan, *ACS Biomaterials Science & Engineering*, 2015, **1**, 271-276.
48. J. Vicente, J. Pinto, J. Menezes and F. Gaspar, *Powder Technology*, 2013, **247**, 1-7.
49. B. Chan, C. Li, K. Au-Yeung, K. Sze and A. Ngan, *Annals of biomedical engineering*, 2008, **36**, 1254-1267.
50. Y.-J. Seong, G. Lin, B. J. Kim, H.-E. Kim, S. Kim and S.-H. Jeong, *ACS Omega*, 2019, **4**, 13834-13844.
51. V. B. Nguyen, C. X. Wang, C. R. Thomas and Z. Zhang, *Chemical Engineering Science*, 2009, **64**, 821-829.
52. R. J. H. Stenekes, S. C. De Smedt, J. Demeester, G. Sun, Z. Zhang and W. E. Hennink, *Biomacromolecules*, 2000, **1**, 696-703.
53. S. Girod Fullana, H. Ternet, M. Freche, J. L. Lacout and F. Rodriguez, *Acta Biomaterialia*, 2010, **6**, 2294-2300.